

Article

Photovoltaic Integrated Hybrid Microgrid Structured Electric Vehicle Charging Station and Its Energy Management Approach

Dominic A. Savio ^{1,*}, Vimala A. Juliet ², Bharatiraja Chokkalingam ¹ ,
Sanjeevikumar Padmanaban ^{3,*} , Jens Bo Holm-Nielsen ³ and Frede Blaabjerg ⁴ 

¹ Department of Electrical and Electronics Engineering, SRM IST, Chennai 603 203, India; bharatiraja@gmail.com

² Department of Electronics and Instrumentation Engineering, SRM IST, Chennai 603 203, India; vimlala@yahoo.co.in

³ Center for Bioenergy and Green Engineering, Department of Energy Technology, Aalborg University, 6700 Esbjerg, Denmark; jhn@et.aau.dk

⁴ Center of Reliable Power Electronics (CORPE), Department of Energy Technology, Aalborg University, 9100 Aalborg, Denmark; fbl@et.aau.dk

* Correspondence: agdominicsavio@gmail.com (D.A.S.); san@et.aau.dk (S.P.); Tel.: +45-716-820-84 (S.P.)

Received: 18 November 2018; Accepted: 29 December 2018; Published: 4 January 2019



Abstract: A hybrid microgrid-powered charging station reduces transmission losses with better power flow control in the modern power system. However, the uncoordinated charging of battery electric vehicles (BEVs) with the hybrid microgrid results in ineffective utilization of the renewable energy sources connected to the charging station. Furthermore, planned development of upcoming charging stations includes a multiport charging facility, which will cause overloading of the utility grid. The paper analyzes the following technical issues: (1) the energy management strategy and converter control of multiport BEV charging from a photovoltaic (PV) source and its effective utilization; (2) maintenance of the DC bus voltage irrespective of the utility grid overloading, which is caused by either local load or the meagerness of PV power through its energy storage unit (ESU). In addition, the charge controller provides closed loop charging through constant current and voltage, and this reduces the charging time. The aim of an energy management strategy is to minimize the usage of utility grid power and store PV power when the vehicle is not connected for charging. The proposed energy management strategy (EMS) was modeled and simulated using MATLAB/Simulink, and its different modes of operation were verified. A laboratory-scale experimental prototype was also developed, and the performance of the proposed charging station was investigated.

Keywords: hybrid microgrid; battery electric vehicle; energy management strategy; vehicle-to-vehicle charging; energy storage unit

1. Introduction

The road transportation sector (RTS) utilizes a substantial proportion of oil and gas resources, produces carbon emissions, and pollutes the environment [1]. To limit the usage of fossil fuels and to reduce CO₂ emissions, an alternate solution has been developed: the battery electric vehicle (BEV) [2,3]. However, problems related to the complete adoption of the BEV, such as the selection of a suitable electric motor drive, power controller, charging facility, battery management system, fast charging system, and coordinated charge management system, need to be resolved [4,5].

Integration of BEVs and renewable energy sources (RESs) with hybrid microgrids is much needed to provide high DC power directly without any reactive power compensation [6,7]. To meet the local

load demand and BEV requirements, the modern charging station needs to be upgraded [8,9]. A BEV charging station powered by photovoltaic (PV) energy produces uncertainties between PV and BEV which can be analyzed by radial distribution systems [10]. The losses from AC-DC conversion can be minimized by selecting the proper operating voltage level at the charging station [11]. Similarly, the number of required charging stations can be significantly reduced by developing multiport charging with real-time forecasting of charging station infrastructure [12,13]. The PV and energy storage unit (ESU)-connected DC microgrid system is used to charge BEVs available at the charging station, and the DC bus connection with the RES has to follow requirements for network coordination, earthing, and DC network protection [14]. A rudimentary multiport BEV charging architecture with a hybrid microgrid is illustrated in Figure 1. It consists of a PV power generating unit, ESU, utility grid, BEV charging points, local load (home appliance), AC-DC-AC bidirectional converter, and bidirectional buck/boost converters.

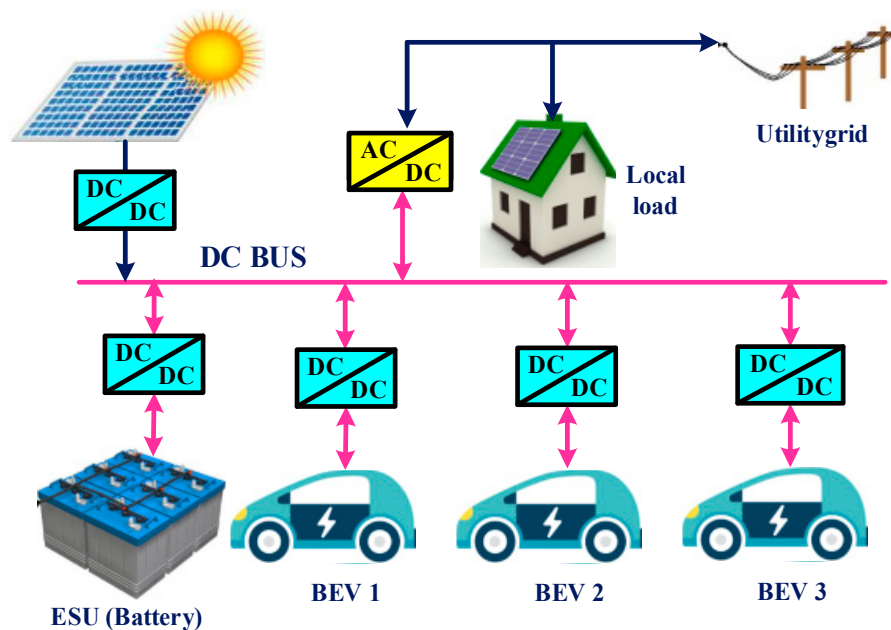


Figure 1. Model of hybrid microgrid battery electric vehicle (BEV) charging station.

In a PV integrated hybrid microgrid, the DC bus power level varies based on the irradiation falling on the PV panel, which creates an unbalance condition in the microgrid [15,16]. The DC microgrid powered by PV and regenerative braking at a railway station with an ESU provides an option to store the available power [17]. The ESU of rechargeable type batteries is used for grid-connected applications because of its modular configuration, moderate energy density, and ability to absorb or deliver appreciable power [18]. Using the MPPT algorithm (incremental conductance method), maximum power from the PV is obtained by changing the switching pulse duration of the boost converter [19]. The bidirectional DC-AC converter provides the power flow from the DC microgrid to the utility grid through reactive power control and grid synchronization [20,21]. The DC-DC charging power converter supplies power with the required voltage to the BEV battery, which increases the overall power conversion efficiency with minimum conversion losses [22]. However, the output voltage level of the DC-DC converter needs to meet the defined standard operating voltage.

Considering the voltage level, EV chargers are classified into three types, namely: DC level 1 (200–450 V, 80 A, up to 36 kW), level 2 (200–450 V, 200 A, up to 90 kW), and level 3 (200–600 V, 400 A, up to 240 kW) [23]. Similarly, the Society of Automotive Engineers (SAE) requirements—namely, SAEJ1772, SAEJ2293, and SAEJ2836—define the operating voltage levels for charging cords and connectors. The proposed multiport hybrid charging station is developed at an operating power of 12 kW by adapting the DC level 1 charging standard and type 1 SAEJ1772 connector [24].

The power conversion efficiency of the charging station is improved by effectively utilizing the generated power with the proper energy management strategy (EMS) technique. The microgrid voltage level is regulated, and the power flow between the microgrid and charging terminals is controlled based on the demand. In [25], the DC bus voltage was maintained using an LCL compensator at the rectifier side to compensate the reactive power. Similarly, to balance the power generation and distribution at the charging station, the proper controller has to be designed by actively tuning the controller parameters [26]. Moreover, under the dynamic variation of DC bus voltage, the conventional PI controller cannot be tuned precisely. It needs an optimization algorithm to achieve automatic voltage balance control, which was implemented using a nonlinear disturbance observer (NDO)-based DC bus voltage control strategy along with a filter circuit [27]. However, power balancing based on the local demand and RES power production has not been addressed. Hence, a coordinated control strategy is needed for DC bus voltage balancing and to meet the load demand. The separate control strategy with two-level bus voltage for the local load and different ratings of EV involves a high investment cost [28]. The economical configuration of BEV charging stations was modeled through the integration of RESs and energy management planning algorithms. Renewable energy integration can not only reduce the charging cost but also reduce the power stress on the utility grid [29–31]. Many previous studies on local grid voltage control methods have adopted droop controller concepts to regulate the bus voltage in the DC microgrid [32–34].

Moreover, the studies mentioned above focused only on DC bus voltage balancing using different control strategies. Instead, the strategy proposed here effectively utilizes available energy sources using EMS algorithms by meeting the demand can bring down the investment cost and maintains the DC bus voltage. In addition, uninterrupted supply for the multiport charging station is also achieved by using vehicle-to-vehicle (V2V) technology. To make use of V2V technology, the charging points need to have a bidirectional converter (BDC) with EMS control. Likewise, the BEV charger has to support bidirectional power flow between one BEV battery to another BEV battery; this reduces the peak price and manages the uninterrupted charging process [35,36]. Nevertheless, V2V power transfer is performed based on the BEV owner's interest, and surplus available energy can be shared with other vehicles or the grid. There are many optimization techniques used in vehicle-to-vehicle charging modes for cost efficiency, minimizing power loss, maximizing discharging revenues, and reducing peak load [37]. Specifically, Oligopoly game and Lagrange duality optimization techniques are used for V2V charging/discharging [38,39]. When the charging station operates in vehicle-to-grid mode, the utility grid integration with the vehicle follows dynamic grid support and a frequency management system [40].

Based on the above discussion, it is observed that a proper EMS algorithm is required for multiport charging stations to obtain efficient power flow. The following are the major contributions of this paper toward the development of an EMS algorithm for the multiport BEV charging station.

- Eleven different modes of energy management strategies are developed for the proposed microgrid to provide continuous power to the BEV charging point.
- When the utility grid is fully loaded and irradiation for PV energy production is low, BEV charging is delayed or temporarily interrupted, and the ESU and vehicle-to-vehicle charging manage the power demand.
- Mathematical power balance equations for all 11 modes are used to analyze the power flow.
- The proposed hybrid multiport charging station with an EMS was developed and simulated through MATLAB/Simulink. Also, an experimental study was carried out for different modes of operation.

The paper is structured as follows: the architecture of the proposed utility grid-integrated charging station is given in Section 2, and the modes of operation of the charging station are discussed in Section 3. The control operation of the power converter and BEV battery charging controller is discussed in Section 4. The simulation was performed using MATLAB/Simulink, and the results are

presented in Section 5. Experimental validation of the simulation results is discussed in Section 6. Conclusions, including the advantages of the proposed system, are presented in Section 7. Symbols and abbreviations are given in the list titled Abbreviations.

2. Proposed Utility Grid-Integrated Charging Station

A detailed block diagram of the charging station is shown in Figure 2. The charging station consists of an MPPT boost converter for the PV system, three bidirectional DC-DC charging converters, a bidirectional DC-AC converter, and an ESU with bidirectional DC-DC converters. The distribution transformer is connected between the microgrid and AC utility grid. The control of a hybrid microgrid depends on the DC bus voltage. The output of the PV system defines the DC bus voltage, and it varies with changes in irradiation level. A variation in DC bus power of between 1500 W and 10 kW is predicted in the analysis. The power produced by the PV system is 12 kW, which is the maximum power required to charge all BEVs and the ESU. When the ESU and BEVs are connected to the charging terminals, the maximum power drawn from the microgrid is 9 kW. When the DC bus power exceeds 9000 W (PV system producing the maximum output), the excess power is sent to the utility grid.

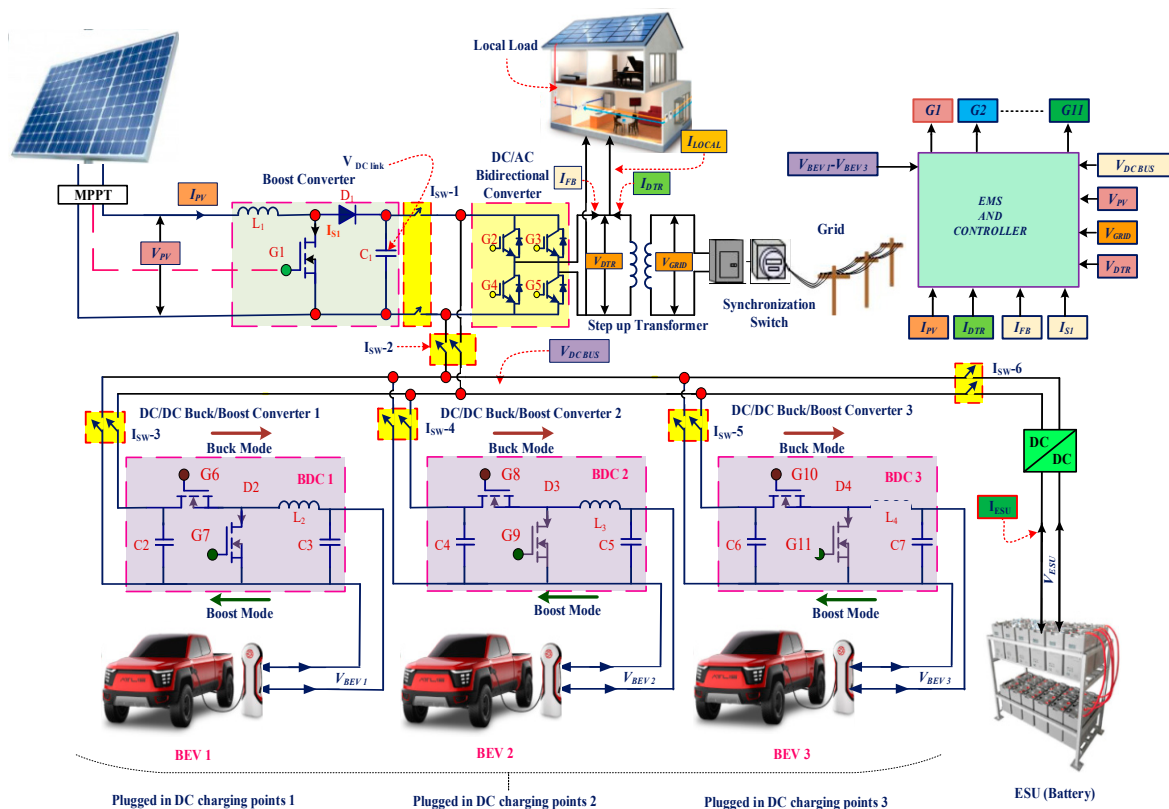


Figure 2. Proposed structure of the utility grid-connected BEV charging station.

Based on the state of charge (SOC) of the three BEVs, the EMS determines the mode of operation, such as grid to vehicle (G2V), ESU to vehicle (ESU2V), and V2V. The BEV operates in V2V mode when there is a demand for electricity in the hybrid microgrid. The operating modes are selected based on the reference DC power produced by PV and distribution transformer current. The 11 operating modes of the charging station and the direction of power flow are depicted in Figure 3.

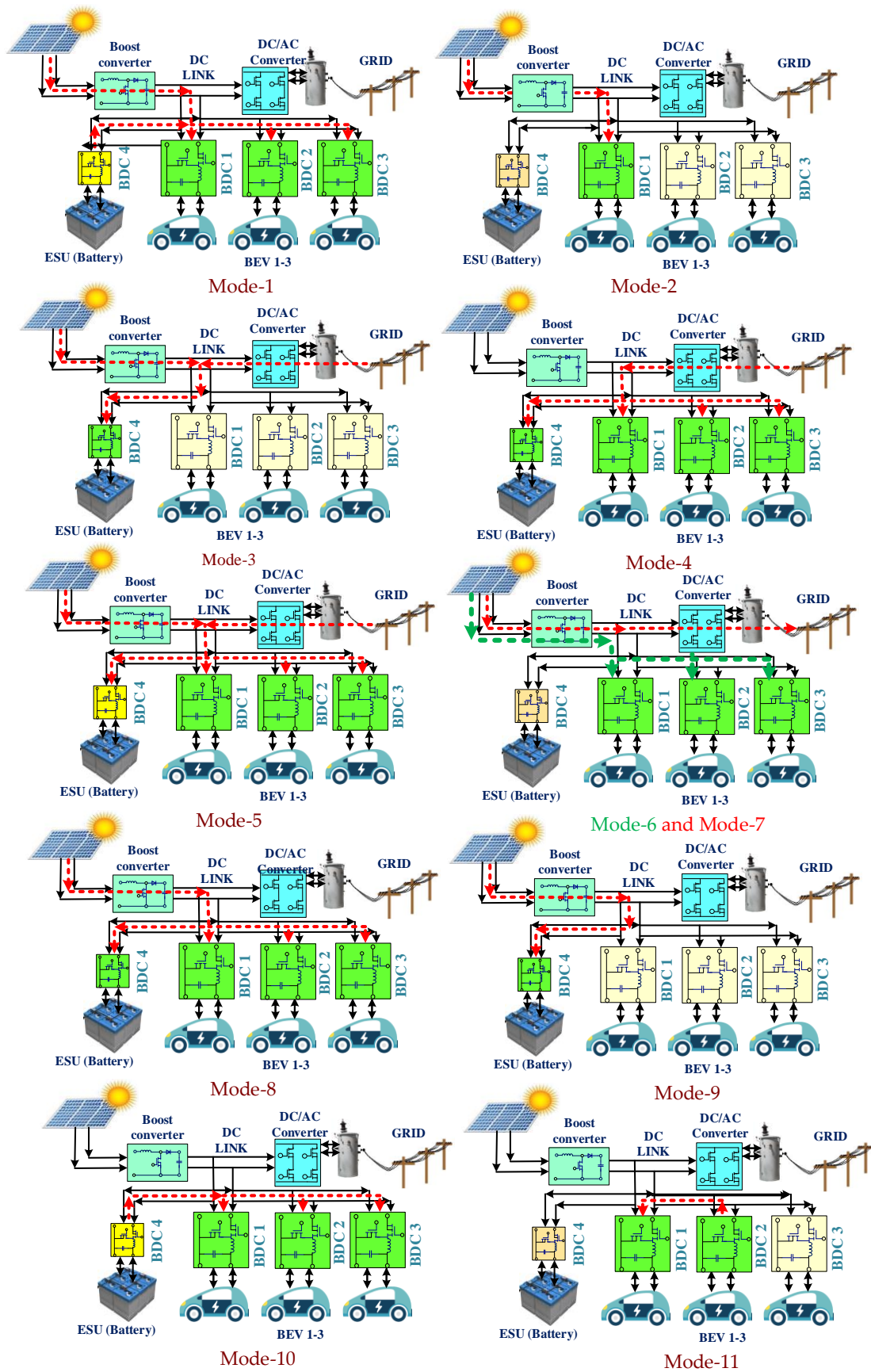


Figure 3. Operating modes of the charging station.

Based on the charging current (I_{ref}), the bidirectional converter operates in buck or boost mode. If I_{ref} is less than or equal to zero, the BEV is fully charged and does not take current from the DC bus; the particular charging bidirectional converter operates in boost mode (V2V). If I_{ref} of the BEV is greater than zero, the BEV needs to be charged; hence, the particular charging bidirectional converter operates in buck (microgrid to vehicle) mode. With BDC 1, BDC 2, and BDC 3 indicating the bidirectional converters, the various combinations of I_{ref} and the operating modes of the bidirectional converters are shown in Figure 4.

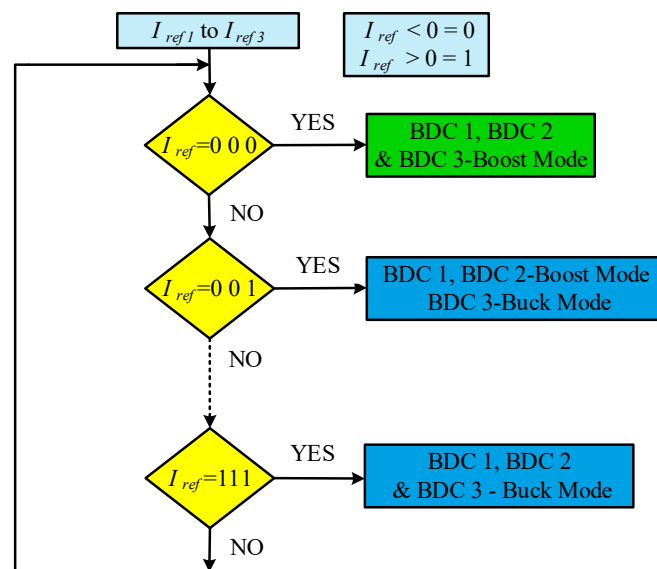


Figure 4. Operating modes of bidirectional converter (BDC).

3. Energy Management Modes of Charging Station

The EMS of the charging station was developed based on various parameters of the charging station to provide a continuous supply to the charging point. The EMS flowchart of the charging station is shown in Figure 5. The following variables are taken into consideration for deciding on the different operating modes: I_{DTR} , P_{PV} , $P_{PV REF-1}$, $P_{PV REF-2}$, $P_{PV REF-3}$, SOC_{ESU} , and SOC_{BEVs} . The various modes and direction of power flow are as follows:

- (1) PV and ESU to BEV charging mode (Mode-1).
- (2) PV to particular BEV charging mode (Mode-2).
- (3) PV and utility grid-connected ESU charging mode (Mode-3).
- (4) PV and utility grid-connected BEV charging mode (Mode-4).
- (5) PV and utility grid-connected ESU and BEV charging mode (Mode-5).
- (6) PV to BEV charging mode (Mode-6).
- (7) PV to grid inversion mode (Mode-7).
- (8) PV to ESU and BEV charging mode (Mode-8).
- (9) PV to ESU charging mode (Mode-9).
- (10) ESU to BEV charging mode (Mode-10).
- (11) BEV to BEV charging mode (Mode-11).

(1) Mode-1: PV and ESU to BEV charging mode

$$P_{PV} < P_{PV REF-1}, I_{DTR} \geq I_{DTR-MAX}, P_{PV} \leq P_{BEV-N} \text{ \& } SOC_{ESU} \geq 40\%$$

During peak demand at the utility grid, the PV system produces the power; nevertheless, it is not sufficient to charge the BEV present at the charging point. Therefore, the power required to

charge the BEV is taken from PV and the ESU. When the power is shared through the DC bus using the bidirectional DC-DC converter, the ESU side's BDC operates in boost mode and the BEV side's BDC operates in buck mode. When the BEV battery charge exceeds the reference SOC, DC-DC buck converters are disconnected from the BEV battery. The power balance equation of the charging station is as follows.

$$P_{CS} = P_{PV} + P_{ESU} - \sum_{N=1}^3 P_{BEV-N} \quad (1)$$

(2) *Mode-2: PV to particular BEV charging mode*

$$P_{PV} < P_{PV\ REF-1}, I_{DTR} \geq I_{DTR-MAX}, SOC_{ESU} \leq 40\% \ \& \ P_{PV} \geq P_{BEV-k}$$

During peak demand at the utility grid, the PV produces power which is sufficient to charge any BEV available at the charging point. Therefore, the BEV is charged from the PV, and the total power balanced in this mode is as follows.

$$P_{CS} = P_{PV} - P_{BEV-k} \quad (2)$$

(3) *Mode-3: PV and utility grid-connected ESU charging mode*

$$P_{PV} < P_{PV\ REF-1}, I_{DTR} \geq I_{DTR-MAX}, 18\% \leq SOC_{ESU} \leq 40\% \ \& \ BEV \text{ is not available}$$

During this mode of operation, the utility grid is under off-peak hours. A BEV is not available at the charging point, and the ESU has the SOC to supply only the local load. Therefore, the utility grid and PV supply the power to charge the ESU, and the total power balanced in this mode is as follows.

$$P_{CS} = P_{PV} + P_{UG} - P_{ESU} \quad (3)$$

(4) *Mode-4: PV and utility grid-connected BEV charging mode*

$$P_{PV} < P_{PV\ REF-1} \ \& \ I_{DTR} \leq I_{DTR-MAX} \ \& \ SOC_{ESU} \geq 40\% \ \& \ P_{PV} < P_{BEV-K}$$

During this condition, the power generated by the PV system is not sufficient to charge a BEV. In this circumstance, the DC bus is powered by both PV and the utility grid. In this mode, utility grid supply is rectified and given to the DC bus through a bidirectional AC/DC converter. The total power balanced in the charging station is as follows.

$$P_{CS} = P_{PV} + P_{UG} - \sum_{N=1}^3 P_{BEV-N} \quad (4)$$

(5) *Mode-5: PV and grid-connected BEV and ESU charging mode*

$$P_{PV\ REF-1} < P_{PV} < P_{PV\ REF-2}, I_{DTR} < I_{DTR-MAX}, \ \& \ , SOC_{ESU} \leq 40\% \ \& \ P_{PV} < P_{BEV-N}$$

During this mode, the power generated by the PV system is not enough to charge all the BEVs and the ESU available at the charging station. Therefore, the power generated from the PV system is given to the microgrid, and the remaining power is obtained from the utility grid. If the distribution transformer draws more current than the reference level due to an increase in local load, to reduce the stress on the distribution transformer, utility grid charging of BEVs has to be terminated. Therefore, the ESU and BEVs are charged from both PV and the utility grid; the total power balanced in this mode is as follows.

$$P_{CS} = P_{PV} + P_{UG} - P_{ESU} - \sum_{N=1}^3 P_{BEV-N} \quad (5)$$

(6) *Mode-6: PV to BEV charging mode*

$$P_{PV\ REF-1} < P_{PV} < P_{PV\ REF-2}, I_{DTR} \geq I_{DTR-MAX}, \& P_{PV} \geq P_{BEV-N}$$

During this mode, the power produced by the PV system is sufficient to charge all the BEVs available at the charging point but not sufficient to charge the ESU. The charging station cannot take any supply from the utility grid, which is in peak demand of electricity. Therefore, a BEV is charged from the PV system, and the total power balanced in this mode is as follows.

$$P_{CS} = P_{PV} - \sum_{N=1}^3 P_{BEV-N} \quad (6)$$

(7) *Mode-7: Utility grid inversion mode*

$$P_{PV\ REF-1} < P_{PV} < P_{PV\ REF-2}, SOC_{ESU} \geq 90\%, SOC_{BEV_s} \geq 90\% \text{ or BEV not available}$$

The power generated by the PV is sufficient to charge all the BEVs at the charging terminals. If BEVs are not available at the charging terminal, the power generated by the PV system is given to the utility grid through the bidirectional DC-AC converter.

$$P_{CS} = P_{PV} - P_{UG} \quad (7)$$

(8) *Mode-8: PV-connected ESU and BEV charging mode*

$$P_{PV\ REF-2} < P_{PV} < P_{PV\ REF-3}, SOC_{ESU} \leq 90\%, BEV\ available\ SOC_{BEV_s} \leq 90\%$$

In this mode, the PV system generates maximum power, and the total power generated by the PV system is sufficient to charge BEVs and the ESU. Therefore, the BEV and ESU are charged from the PV system, and the total power balanced in this mode is as follows.

$$P_{CS} = P_{PV} - P_{BEV} - P_{ESU} \quad (8)$$

(9) *Mode-9: PV to ESU charging Mode*

$$P_{PV\ REF-3} \geq P_{PV} \& I_{DTR} \geq I_{DTR-MAX}, SOC_{ESU} \leq 90\% \& SOC_{BEV} \geq 90\%$$

In this mode, the power generated by the PV system is sufficient to charge BEVs and the ESU. All the BEVs are fully charged and the SOC of ESU is less than 90%. All the power generated from the PV system is given to the microgrid to charge the ESU. Therefore, the ESU is charged from the PV system, and the total power balanced in this mode is as follows.

$$P_{CS} = P_{PV} - P_{ESU} \quad (9)$$

(10) *Mode-10: ESU to BEV charging mode*

$$I_{DTR} \geq I_{DTR-MAX}, SOC_{ESU} \geq 90\%, P_{PV} < P_{PV\ min}, SOC_{ESU} \leq 90\% \text{ and BEV available for charging}$$

In this mode, the PV system is not generating power due to low irradiation and bad weather conditions. The utility grid is overloaded due to the local load demand, the BEVs are charged using ESU, and the total power balanced in this mode is as follows.

$$P_{CS} = P_{ESU} - \sum_{N=1}^3 P_{BEV-N} \quad (10)$$

(11) Mode-11: Vehicle-to-Vehicle (V2V) mode

$$I_{DTR} \geq I_{DTR-MAX}, SOC_{BEV} \geq 90\%, P_{PV} < P_{PV\ min}, SOC_{ESU} \leq 40\% \text{ and BEV available for charging}$$

In this mode, the PV system is not generating power due to low irradiation and bad weather conditions. The utility grid is overloaded due to the local load, the ESU has the SOC to supply only the local load, and the BEVs are charged using nearby BEVs. The total power balanced in this mode is as follows.

$$P_{CS} = P_{BEV-2} - P_{BEV-1} \tag{11}$$

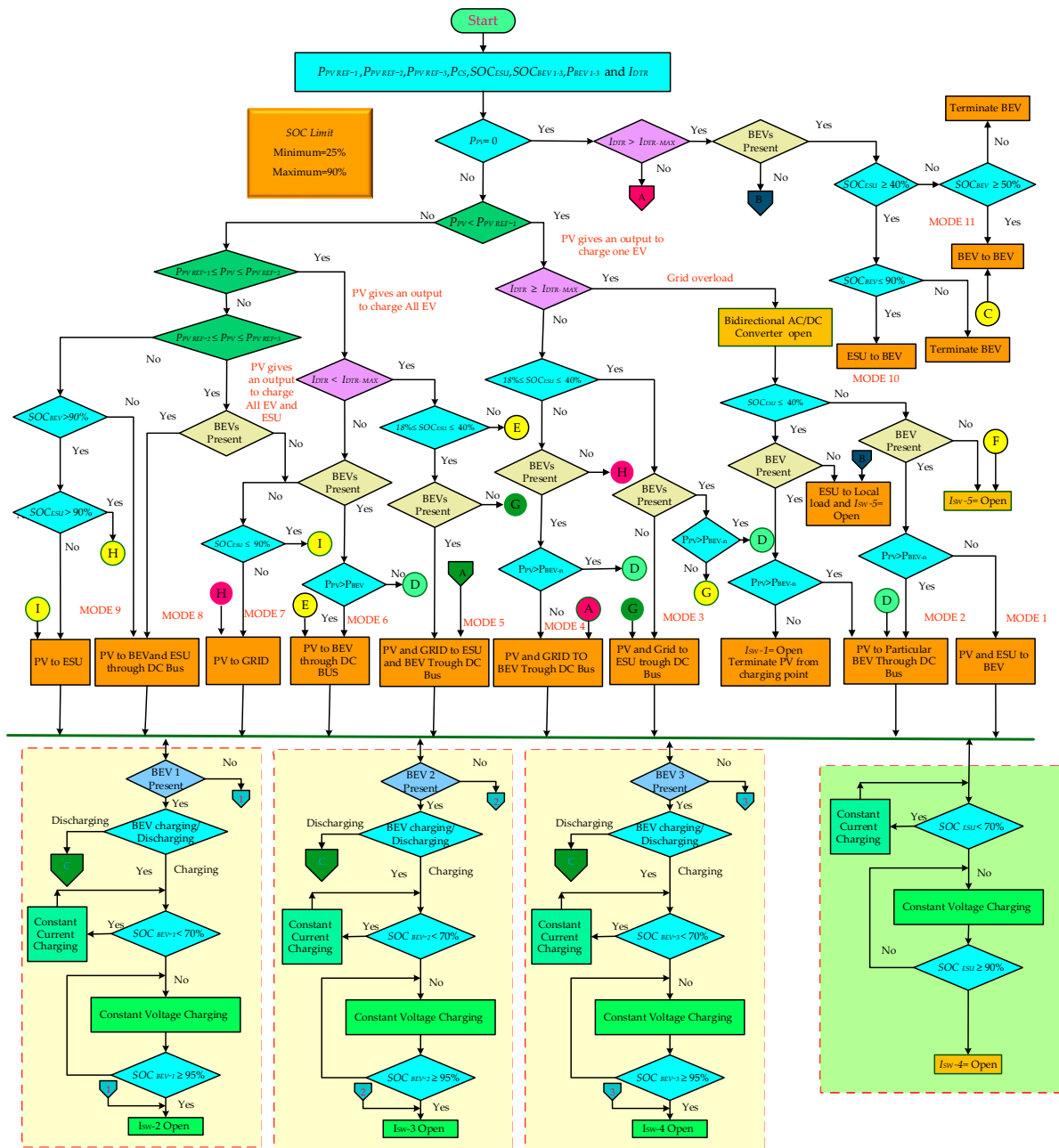


Figure 5. The flowchart for the charging station energy management strategy (EMS).

4. Control Operation of Power Converters

The switching sequence of all the power electronic converters is controlled based on different parameters that are measured from the DC bus and the charging station-connected vehicle. The PV side's MPPT DC-DC converter is controlled based on the voltage and current that are measured from the PV devices. The BEV side's buck/boost converter to be controlled is based on the state of charge and the current drawn by the battery.

BEV Battery Charging Controller

The BEV battery is charged by providing constant-voltage and constant-current control to the charging converter. Fast charging is done by inner current loop control; the outer voltage loop control used for constant-voltage charging is shown in Figure 6. When the current flowing into the battery is positive, $I_{batt} > 0$, the battery is charged; otherwise, it is discharged. Based on the sign of the battery current (I_{ref}), the EMS controller is providing regulated supply to the battery.

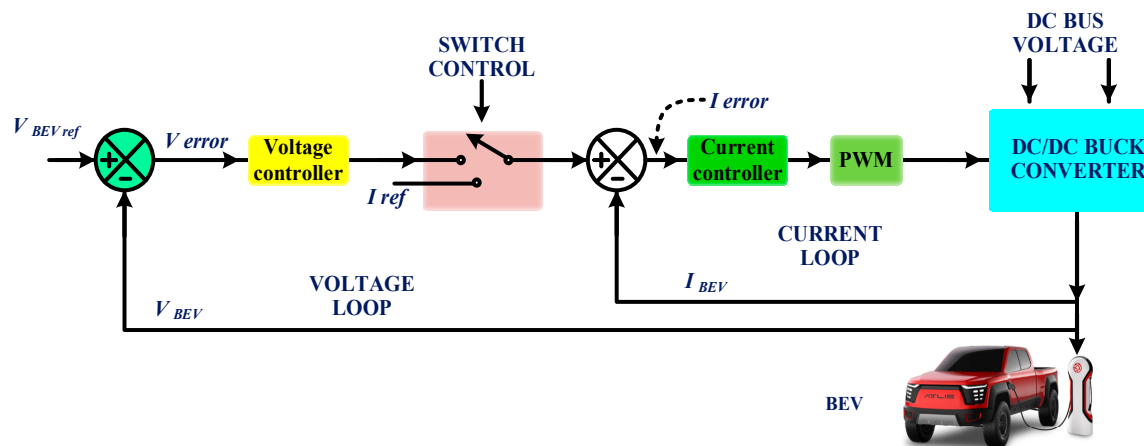


Figure 6. Charging and discharging of a BEV battery.

Depending on the SOC and sign of the reference current (I_{ref}), the charging converter operates under different modes. Based on the control signal, it can be operated under constant-current or constant-voltage mode. When the switch is open, the charging station converter operates in constant-current charging mode; if the switch is closed, the charging station converter operates in constant-voltage charging mode.

5. Simulation and Evaluation of Charging Station

Different modes of the charging station were evaluated using MATLAB Simulink. The simulation module consists of the BEV battery and power converters: DC-AC, AC-DC, and DC-DC converters. A PV system of 12 kW and the utility grid are used to power the charging station. A backup ESU battery of 6 kWh (48 V) is connected to the charging station to provide uninterrupted supply. The BEVs are considered to be storage batteries (BEV 1–3) with a power rating of 1 kW.

The reference DC bus power, current, and SOC values for all DC microgrid-to-vehicle modes of the charging station are as follows: $P_{PV\ MAX} = 12\ kW$, $P_{PV\ MIN} = 1.5\ kW$, $I_{DTR\ MIN} = 12\ A$, $I_{DTR\ Max} = 17.5\ A$, $SOC_{MIN} = 18\%$, and $SOC_{MAX} = 90\%$. The DC bus voltage and power generated by the PV system varies with the change in irradiation from the sun. The PV system starts to deliver power when the DC bus voltage is greater than 50 V. The PV system yields 250 V, and the power of the DC bus is 7.5 W, which is required to charge both the energy storage unit and electric vehicles. The DC bus power is greater than 10 kW (300–320 V) and exceeds the power requirement of the charging station. The different operating modes of the charging station are chosen based on the DC bus power. Using the PV voltage and DC bus power, three threshold values were chosen: $P_{PV\ REF-1} = 1.5\ kW$,

$P_{PV\ REF-2} = 7.5$ kW, and $P_{PV\ REF-3} = 10$ kW. Based on the reference PV power, the charging station is controlled in 11 modes (Mode-1–11).

When the PV power is less than 1.5 kW, the peak demand from the utility grid ($I_{DTR\ MAX} = 17.5$ A) and the ESU have an SOC of greater than 40%; power produced by the PV is not sufficient to charge all the BEVs available at the charging terminals. During this condition, the power required to charge the BEVs is drawn from PV and the ESU, as shown in Figure 7. In Mode-1, total power in the DC bus is maintained as 5.3 kW, which is sufficient to charge all BEVs. With the same PV power level, the charging station has one BEV for charging, and the power produced by the PV system is greater than that needed by the vehicle available at the charging point; the particular BEV is charged from the PV by Mode-2 and is shown in Figure 8.

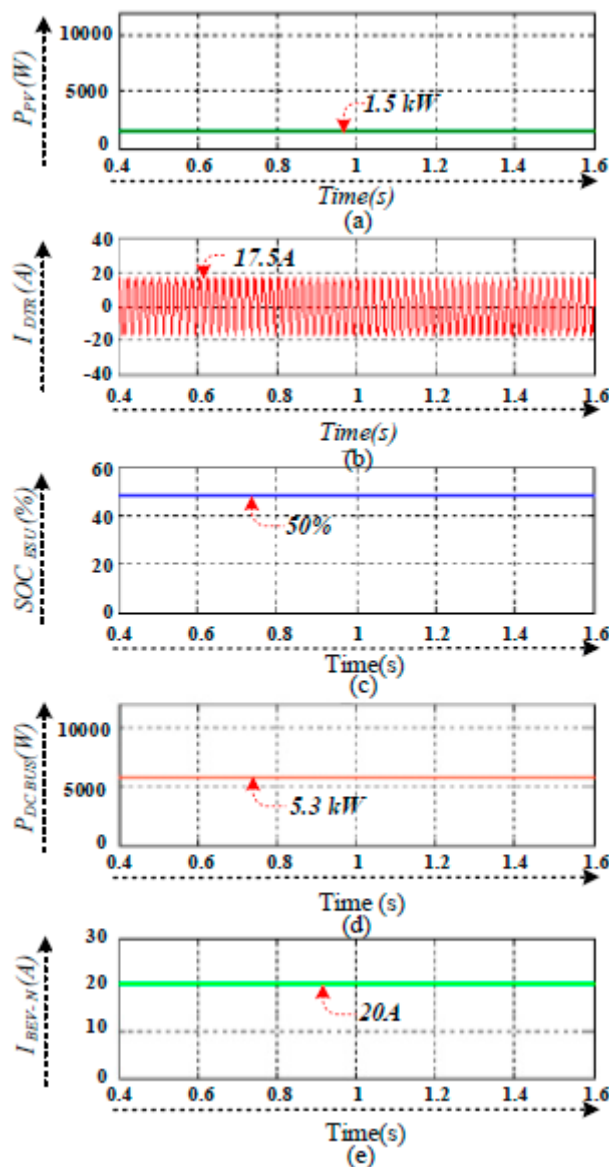


Figure 7. Simulation output of Mode-1: (a) photovoltaic (PV) power, (b) distribution transformer current, (c) state of charge (SOC) of the energy storage unit (ESU), (d) DC bus power, and (e) output current of all of the BEV side's buck converters.

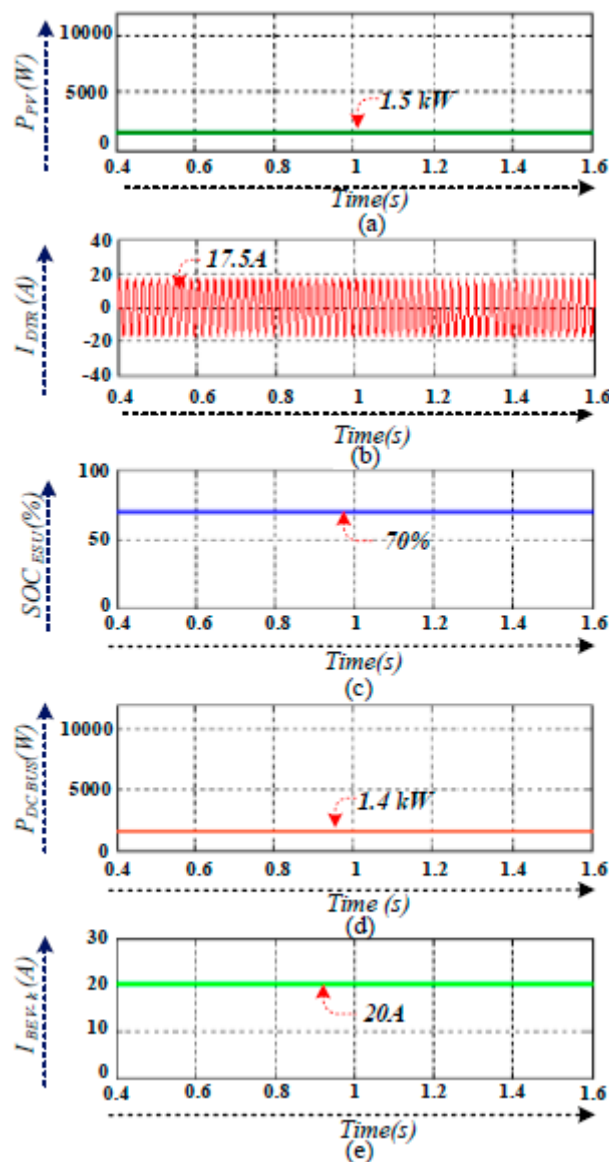


Figure 8. Simulation output of Mode-2: (a) PV power, (b) distribution transformer current, (c) SOC of ESU, (d) DC bus power, (e) output current of any one of the BEV side's buck converters.

When the P_{PV} is less than 1.5 kW, the utility grid is off-peak ($I_{DTR} = 12$ A), the SOC of the ESU is less than 40%, and the power required to charge the ESU and BEVs is drawn from the PV system and the utility grid; the grid-connected AC-DC converter works in rectification mode. Therefore, the ESU and BEVs are charged from the utility grid and PV, and power at the DC bus is maintained at a rated capacity of 11.2 kW; in this scenario, 1.5 kW of power is drawn from the PV and the remaining power is taken from the utility grid, as shown in Figure 9. At the same PV power level, SOC_{ESU} is greater than 40%, and the PV system and the utility grid provide the continuous supply to the charging station. DC bus power is maintained at 11.2 kW, as shown in Figure 10.

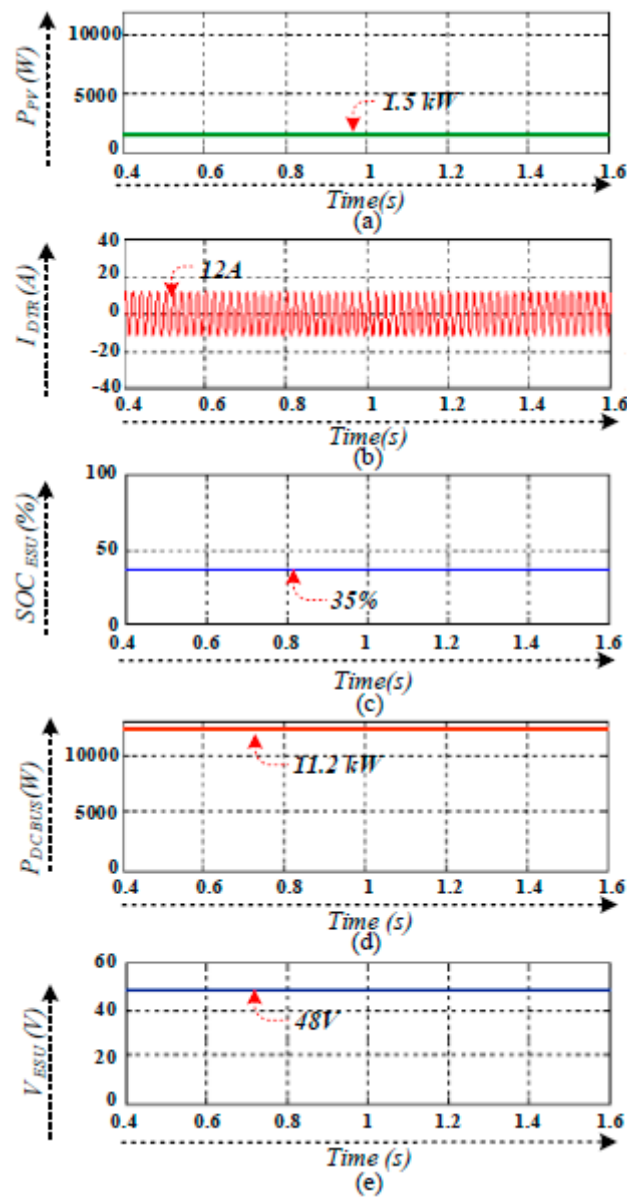


Figure 9. Simulation output of Mode-3: (a) PV power, (b) distribution transformer current, (c) SOC of the ESU, (d) DC bus power, (e) output voltage from the ESU.

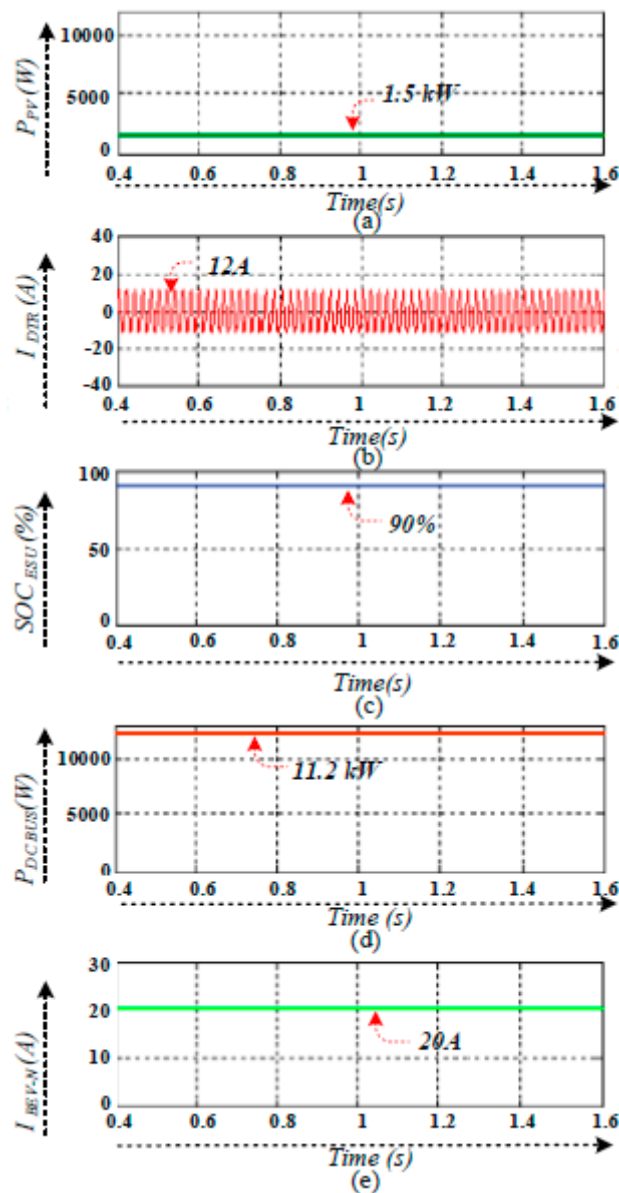


Figure 10. Simulation output of Mode-4: (a) PV power, (b) distribution transformer current, (c) SOC of the ESU, (d) DC bus power, (e) output current of all BEV side's buck converters.

The power generated by the PV system is 7.5 kW, the utility grid is not overloaded, and the SOC of the ESU is less than 40%. The power required to charge the BEV and ESU is 9 kW; all the power generated by the PV is transferred to the DC bus and the utility grid supplies the deficit. Power in the DC bus is maintained at 11.2 kW, as shown in Figure 11. For the above PV power level, the utility grid is at peak conditions; all the BEVs are charged from the PV system, and the DC bus power is maintained at 7.1 kW, as shown in Figure 12.

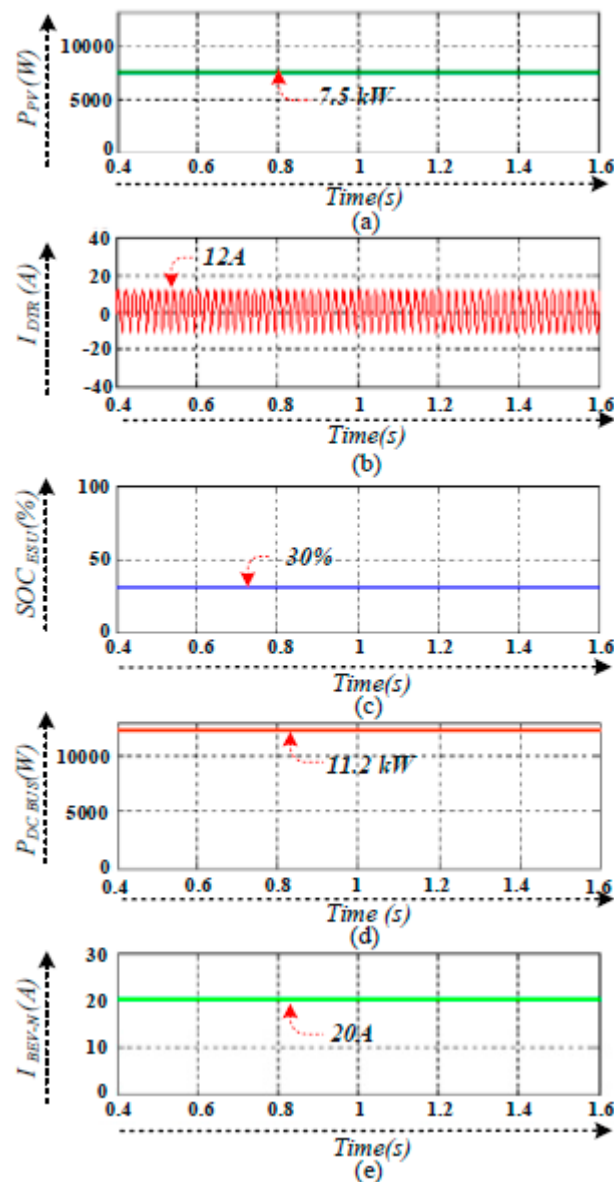


Figure 11. Simulation output of Mode-5: (a) PV power, (b) distribution transformer current, (c) voltage of the ESU, (d) DC bus power, (e) output current of all BEV side's buck converters.

The power generated by the PV system is 7.5 kW or 10 kW, the SOC of the ESU is greater than 90%, and BEVs are not available for charging; the generated PV power is fed back to the utility grid and the DC bus power is maintained at 7.1 kW, as shown in Figure 13. The power generated by the PV system is 10 kW, which is sufficient to charge BEVs and the ESU; DC bus power is maintained at 9.5 kW, as shown in Figure 14.

The power produced by the PV system is 10 kW, and the ESU and BEVs need charging; the DC bus power is maintained at 9.5 kW, as shown in Figure 15. When the PV power is less than 1.5 kW, the SOC of the ESU is greater than the 40%, and BEVs are charged from the ESU; the DC bus power is maintained as 4.8 kW, as shown in Figure 16.

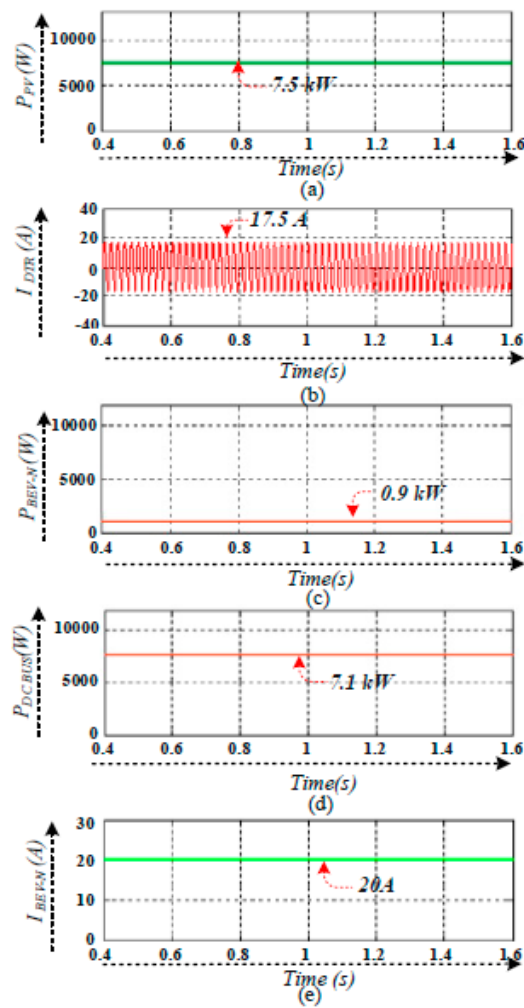


Figure 12. Simulation output of Mode-6: (a) PV power, (b) distribution transformer current, (c) output power of all of the BEV side’s buck converters, (d) DC bus power, (e) output current of all of the BEV side’s buck converters.

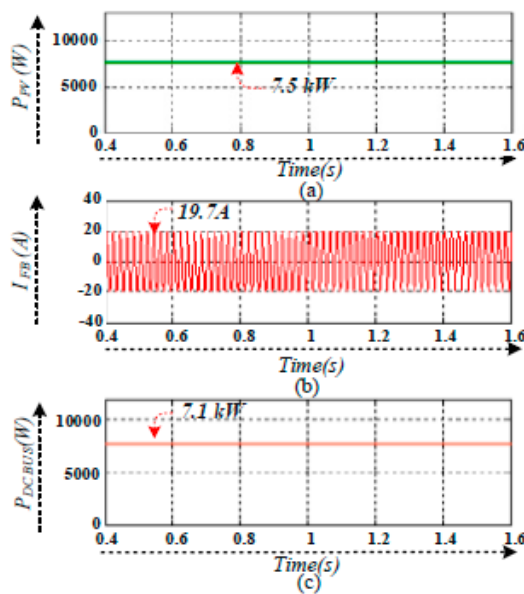


Figure 13. Simulation output of Mode-7: (a) PV power, (b) feedback current to the utility grid, (c) DC bus power.

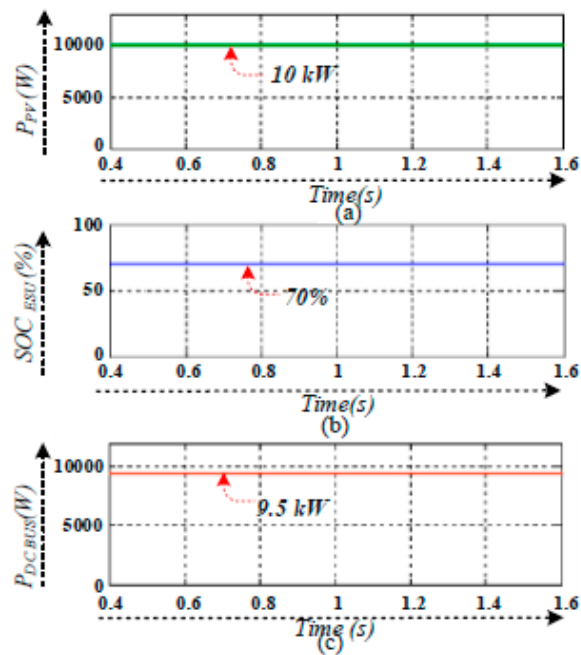


Figure 14. Simulation output of Mode-9: (a) distribution transformer current, (b) SOC of the ESU (c) DC bus power.

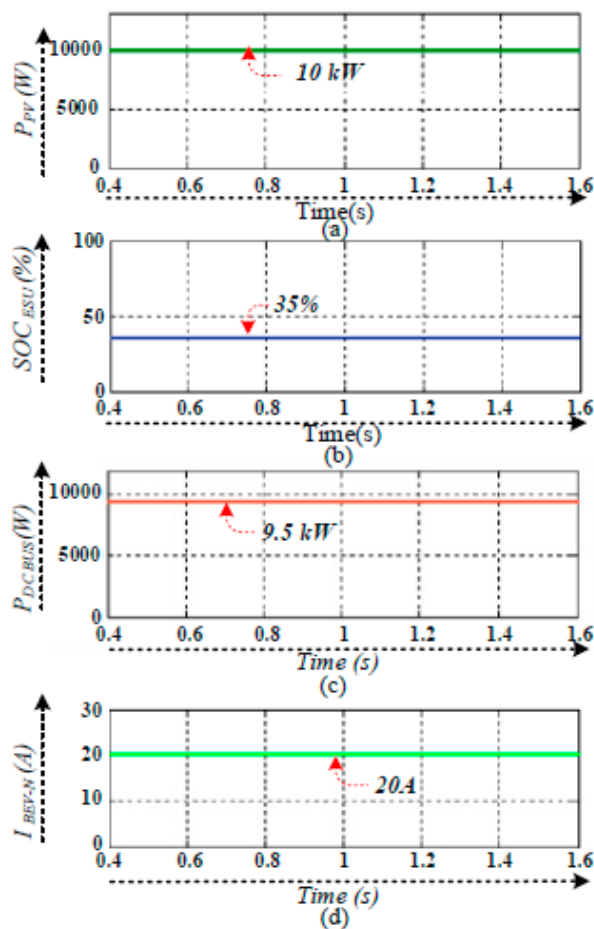


Figure 15. Simulation output of Mode-8: (a) PV power, (b) SOC of the ESU, (c) DC bus power, (d) output current of all of the BEV side's buck converters.

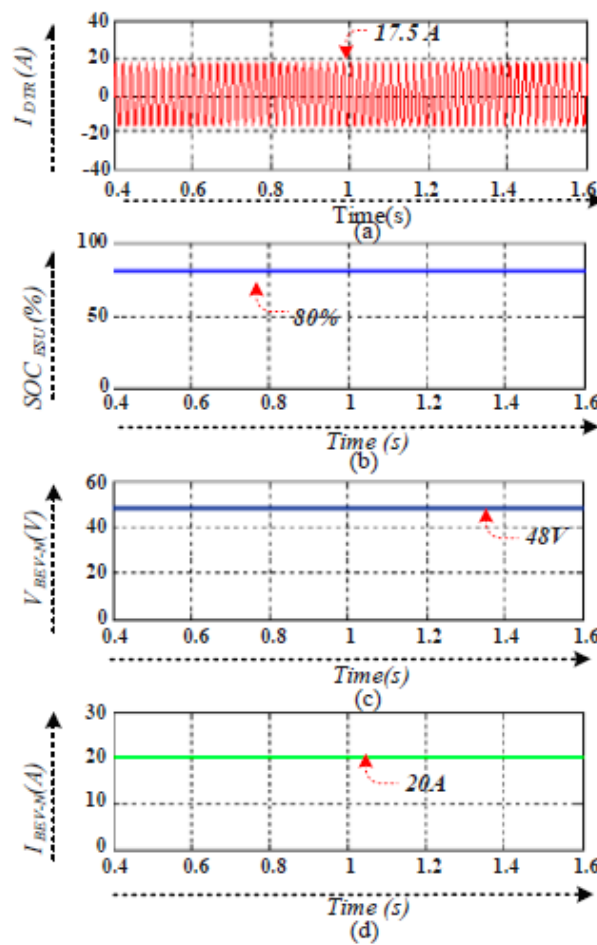


Figure 16. Simulation output of Mode-10: (a) distribution transformer current, (b) SOC of the ESU, (c) output voltage of all of the BEV side’s buck converters, (d) output current of all of the BEV side’s buck converters.

The PV system is not producing any output, the utility grid is overloaded, the SOC of the ESU is less than 40%, and a BEV is charged from other BEVs. Depending upon the price and power demand at peak time, the owner of the BEV has to decide how much power they wish to share with other vehicles. The power flows from one BEV to the other. The amount of power to be sold is identified by the discharge current of the BEV battery; BEV 1 discharges and gives power to BEV 2, as shown in Figure 17.

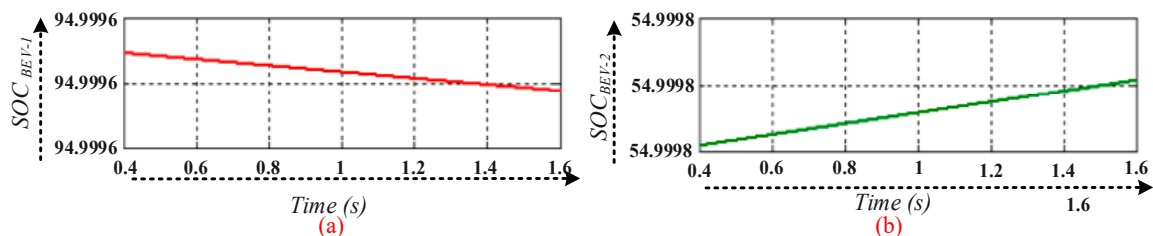


Figure 17. Simulation output of Mode-11: (a) SOC of BEV 1, (b) SOC of BEV 2.

The comprehensive simulation studies demonstrate the power level of the charging station in the different modes. The BEVs are able to charge/discharge based on user requirements. The objective is to obtain superior performance under both steady and variable charging and discharging conditions. By operating the EMS within its rated range, the proposed control system can handle the control needs of the charging station when the physical constraints of power converters are exceeded. At the

end of the case study, it is observed that PV-produced power is effectively used for BEV charging. The different simulation outputs are presented in Table 1. Despite the variations in PV power, the DC grid provides sufficient power for BEV charging through its scattered energy sources. When the PV system provides power of 1500 W and the utility grid is overloaded (17.5 A), the charging station is operated in Mode-1 and -2. In Mode-1, all the BEVs are available for charging and receive power from the PV system and ESU, and the DC grid power is maintained at 5340 W. Similarly, with the above condition, only one BEV is available at the charging terminal (Mode-2); DC grid power is maintained at 1425 W, which is sufficient to charge a particular BEV without receiving power from the ESU.

Table 1. Simulation results of Mode-1–11.

CS Parameters	Mode-1	Mode-2	Mode-3	Mode-4	Mode-5	Mode-6	Mode-7	Mode-8	Mode-9	Mode-10	Mode-11
P_{PV} (W)	1500	1500	1500	1500	7500	7500	7500	10,000	10,000	0	0
I_{DTR} (A)	17.5	17.5	12	12	12	17.5	19.7	NC	NC	17.5	17.5
SOC_{ESU} (%)	50	70	35	90	30	NC	90	35	70	80	25
I_{ESU} (A)	12	NC	12	NC	120	NC	NC	120	120	15	NC
$P_{DC-GRID}$ (W)	5340	1425	11250	11250	11250	7125	7125	9500	9500	4800	1000
P_{BEV-N} (W)	1000	1000	NA	1000	1000	960	NA	1000	FC	1000	950
I_{BEV-N} (A)	20	20	NA	20	20	20	NA	20	FC	20	19

$V_{PV} = 120$ V, $V_{DC\ BUS} = 320$ V, POWER BEV 1–3 = 1 KW, $P_{ESU} = 6$ kWh, NC—Not considered, FC—Fully Charged, NA—Not Available.

6. Experimental Validation

To verify the practical feasibility and effectiveness of the proposed energy management control strategies, experimental tests were carried out in the laboratory. The laboratory prototype of the proposed BEV charging station with a hybrid microgrid was developed for a power of 240 W, as shown in Figure 18. An FPGA controller was used for controlling the overall charging station. The charging station consisted of a PV panel with a single-switch MPPT boost converter, bidirectional buck-boost converter, bidirectional AC-DC converter, and a 12 V, 80 Ah battery (instead of a BEV). The maximum power from the PV (when there is full irradiation) was defined as 240 W ($V_{PV} = 18$ V, $I_{PV} = 13.34$ A). The P&O MPPT algorithm was used with a boost converter to extract the maximum power from the PV system. The mode selection was chosen in a manner similar to that in the simulation study to deal the different cases of PV generation and BEV load connectivity. The charging station was modeled at lab scale, so losses were negligible. However, voltage and power losses of 5% were considered while designing the original system.

The variation in solar irradiation affects the PV power and DC bus voltage. By considering these variations, three power levels were chosen for deciding operating modes. The following threshold values were chosen: $P_{PV\ REF\ 1} = 120$ W, $P_{PV\ REF\ 2} = 160$ W, and $P_{PV\ REF\ 3} = 230$ W. Based on the reference PV power, the charging station was operated in the following modes.

- (1) PV and ESU to BEV charging mode ($P_{PV} \leq 120$ W).
- (2) PV to particular BEV charging mode ($P_{PV} \leq 120$ W).
- (3) PV and utility grid-connected ESU charging mode ($P_{PV} \leq 120$ W).
- (4) PV and utility grid-connected ESU and BEV charging mode ($P_{PV} \leq 120$ W).
- (5) PV and utility grid-connected BEV charging mode ($120\ W \leq P_{PV} \leq 160$ W).
- (6) PV to BEV charging mode ($120\ W \leq P_{PV} \leq 160$ W).
- (7) PV to grid inversion mode ($120\ W \leq P_{PV} \leq 160$ W).
- (8) PV to ESU and BEV charging mode ($160\ W \leq P_{PV} \leq 230$ W).
- (9) PV to ESU charging mode ($P_{PV} \geq 230$ W).
- (10) ESU to BEV charging mode ($P_{PV} < P_{PV\ MIN}$).
- (11) BEV to BEV charging mode ($P_{PV} < P_{PV\ MIN}$).

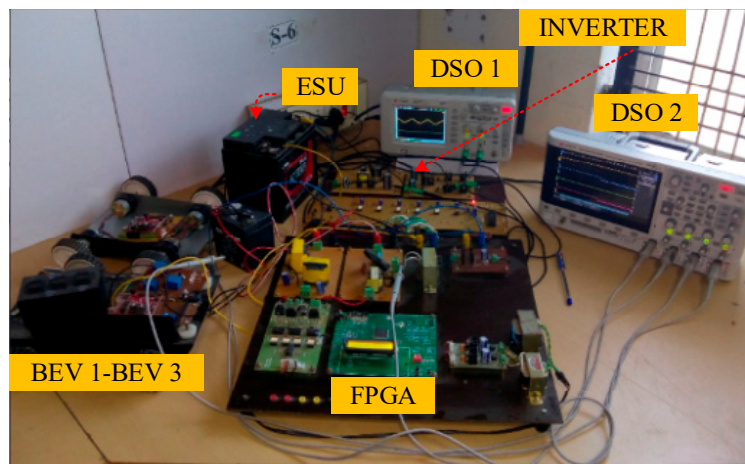


Figure 18. Experimental setup.

When the PV system delivers power of 120 W, with various conditions of the ESU, BEV, and utility grid, the charging station is operated at four modes (Mode-1–4). The BEV is the only load for the first two modes, and in Mode-3 and Mode-4, the BEV and ESU act as the load. Among the first two modes, Mode-2 is taken into consideration to demonstrate the charging current and input power. Similarly, Mode-4 is presented from among Mode-3 and Mode-4.

(1) *Experimental results of Mode-2: PV to particular BEV charging mode ($P_{PV} \leq 120$ W)*

In Mode-2, the PV system provides output that can charge only one BEV, and the DC-DC buck converter gives its output to the BEV battery ($V_{BEV-1} = 12$ V and $I_{BEV-1} = 2.96$ A). The corresponding DC bus power, charging voltage, and current are shown in Figure 19.

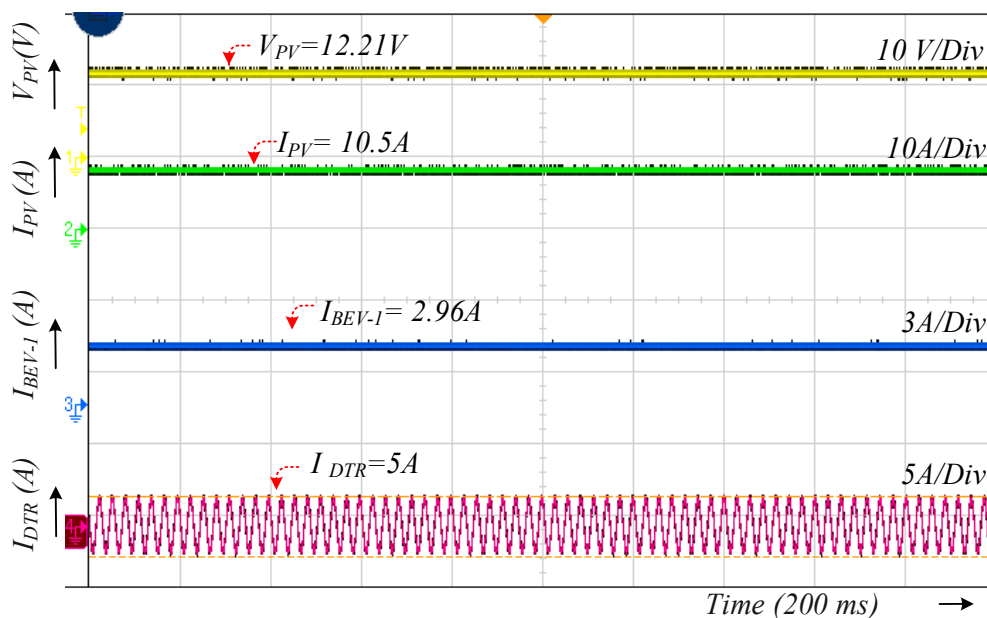


Figure 19. Experimental result of Mode-2: PV charging and utility grid-connected charging.

(2) *Experimental results of Mode-4: PV and utility grid-connected ESU and BEV charging mode ($PPV \leq 120$ W)*

In this mode, the PV system generates power of 120 W, which is not sufficient to charge all the BEVs available at the charging point. Hence, power is drawn from the PV system and utility grid. The voltage and current are delivered from the PV system ($V_{PV} = 12.21$ V and $I_{PV} = 10.54$ A); the current drawn from the distribution transformer is 2 A, which is shown in Figure 20.

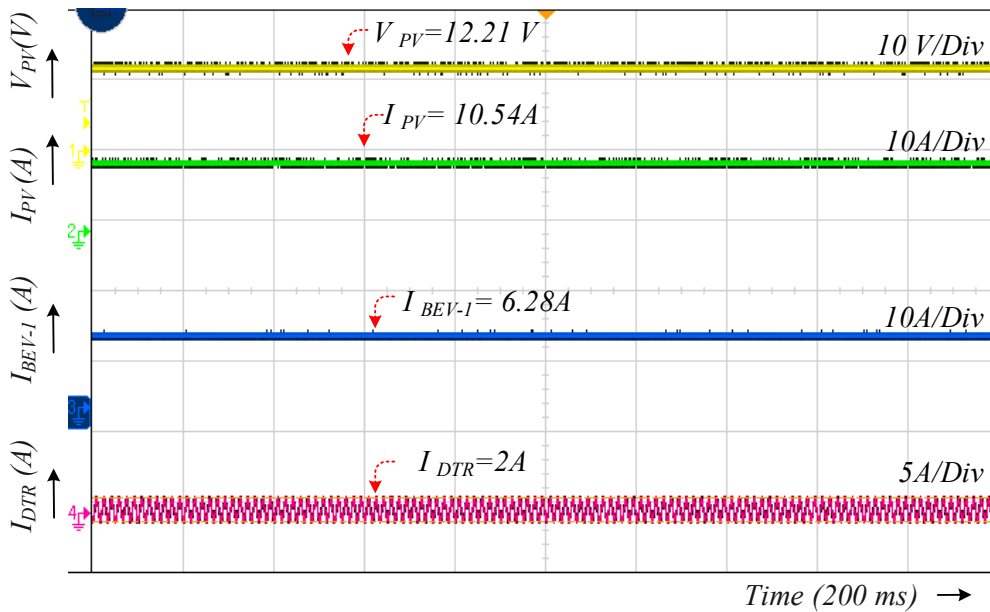


Figure 20. Experimental result of Mode-4: PV charging and utility grid-connected charging.

From Mode-5 to Mode-8, the PV system provides power of 120–160 W; among this series, Mode-6 is used for practical demonstration. In Mode-6, the PV system provides power of 150 W for charging all the BEVs available at the charging station. In Mode-8, the PV system provides power of above 160 W, and the ESU and BEV are charged with maximum charging current.

(3) Experimental results of Mode-6: PV to BEV charging mode ($120\text{ W} \leq P_{PV} \leq 160\text{ W}$)

In this mode, the PV system delivers power with the moderate output of the PV panel, which is 150 W ($V_{PV} = 13.09\text{ V}$, $I_{PV} = 11.53\text{ A}$). The DC bus voltage is maintained at 22 V by a PV boost converter. The output of the bidirectional converter in buck mode provides a charging current to BEVs ($V_{BEV1} = 13\text{ V}$, $I_{BEV1} = 3.3\text{ A}$), as shown in Figure 21.

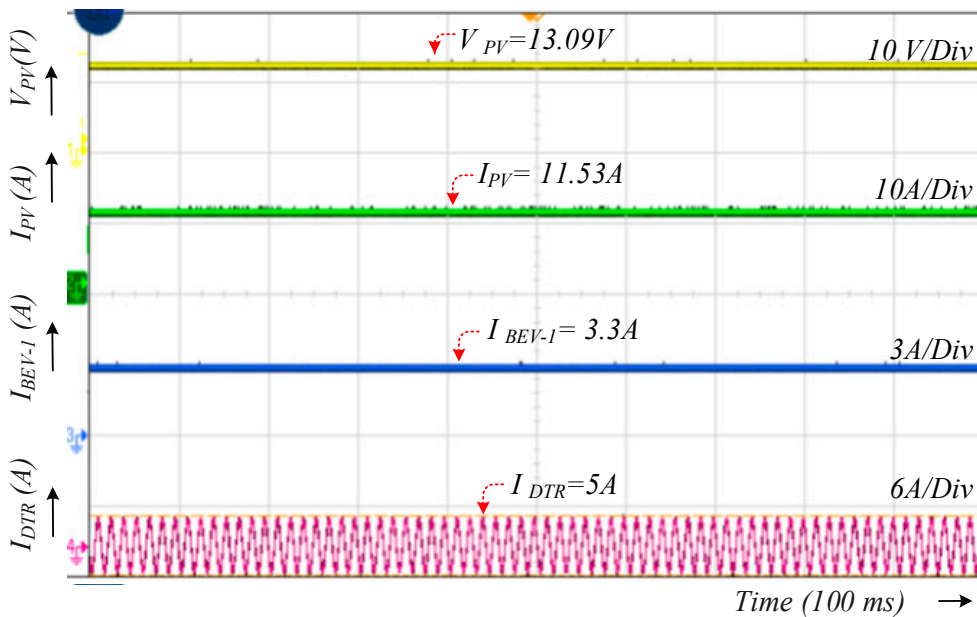


Figure 21. Experimental result of Mode-6: PV to BEV charging mode ($120\text{ W} \leq P_{PV} \leq 160\text{ W}$).

(4) Experimental results of Mode-9: PV to ESU charging Mode ($P_{PV} \geq 230$ W)

This mode is considered to be an energy saving mode; the maximum power delivered by the PV system ($V_{PV} = 18.1$ V, $I_{PV} = 12.7$ A) when BEVs are not available for charging is stored in ESU. A charging voltage of 13.6 V with 4.67 A is used to charge the ESU, as shown in Figure 22.

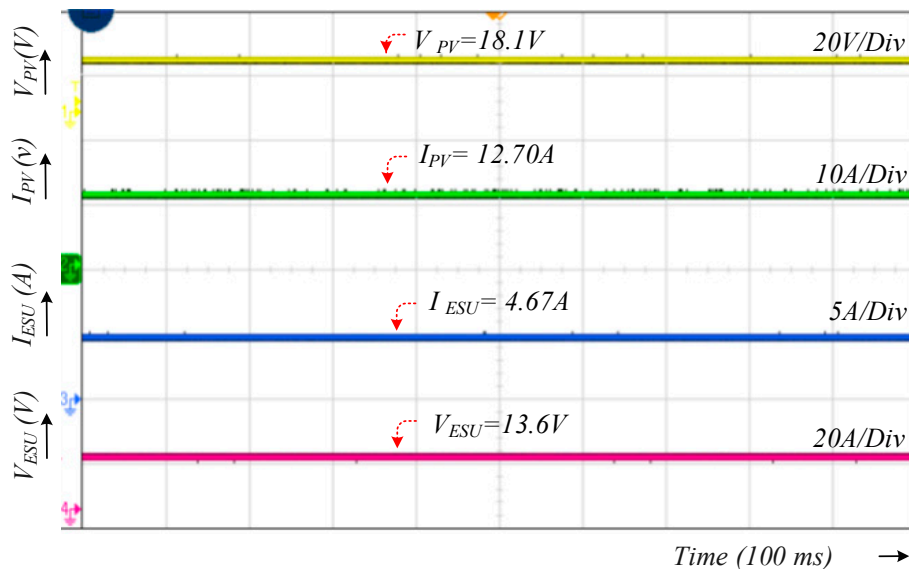


Figure 22. Experimental result of Mode-9: PV to ESU charging mode ($P_{PV} \geq 230$ W).

(5) Experimental results of Mode-10: ESU to BEV charging mode ($P_{PV} = P_{PV\ MIN}$ W)

In this mode, the charging power is transferred from the ESU to BEVs. The PV system and utility grid are not able to provide charging power; the ESU provides a charging supply of 14.1 V and 3.1 A to the BEVs. A BEV is charged with 13.6 V and 2.79 A, as shown in Figure 23.

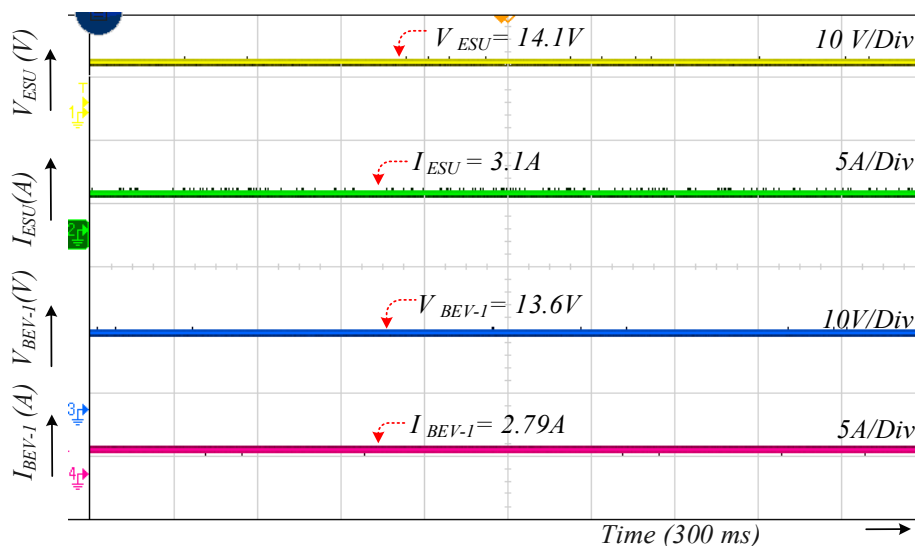


Figure 23. Experimental result of Mode-10: ESU to BEV charging mode ($P_{PV} = 0$ W).

(6) Experimental results of Mode-11: BEV to BEV charging mode ($P_{PV} = P_{PV\ MIN}$ W)

This is the special mode (no power from the PV, utility grid, or ESU) among the 11 modes: a particular BEV is ready to transfer power to another BEV, and there is a power exchange between two

BEVs. The power provided from BEV 1 to BEV 2 is 13.9 V with a current of 1.9 A, and BEV 2 receives a charging supply of 13.8 V with a current of 1.81 A, as shown in Figure 24

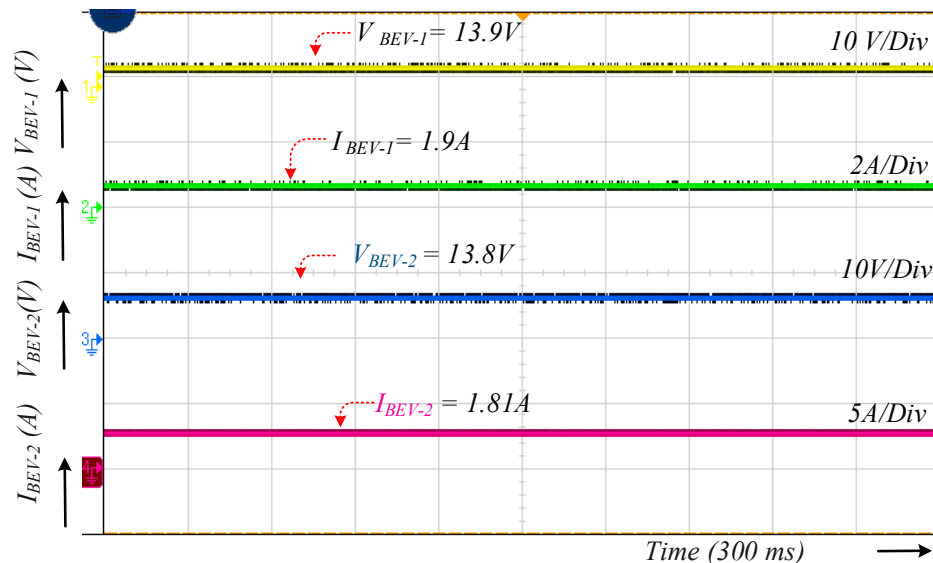


Figure 24. Experimental result of Mode-11: BEV to BEV charging mode ($P_{PV} < P_{PV\ MIN}$ W).

The different operating modes mitigate the loading of the distribution transformer and provide an uninterrupted supply to the charging station. This infrastructure with an EMS is suitable for workplace-based RES charging. In these different modes, PV-generated power is effectively used for charging. For example, in Mode-2, the PV-generated power is sufficient to charge any one BEV available at the charging point effectively. In Mode-4, PV-generated power is insufficient to charge the ESU and BEV; thus, the charging station receives power from the utility grid. Similarly, other modes provide uninterrupted power for charging a BEV through this energy management approach.

Table 2 compares pros and cons of the proposed charging station with proposed strategies from other published papers. From the table, it can be seen that the proposed charging infrastructure and its energy management can potentially utilize PV power to realize a continuous EV charging facility.

Table 2. Comparison of charging stations.

Ref. Papers	Microgrid Type	On board Storage System	Nonrenewable Sources Connected	Renewable Sources	Utility Grid Connected	Type of Charging	Control Strategy	V2V Charging	Pros and Cons
[41]	AC	YES	Two Diesel Generators	PV	YES	On board	Load demand	YES	Pros: ● Generators used; Uninterrupted supply Cons: ● Conversion needs for charging
[42]	Hybrid	YES	NO	PV and WIND	YES	On board	Power Control	NO	Pros: ● High power density converter used for charging Cons: ● PV to grid stabilize the demand
[43]	DC	YES	NO	PV	YES	Off board	DC link voltage	NO	Pros: ● Distribution Transformer upgradation not required Cons: ● Not used ESU for store PV power
[44]	AC	YES	NO	NO	YES	Off board	Power Control Strategies	NO	Pros: ● Smart charging Cons: ● AC distribution network, increases conversion losses
[45]	DC	NO	NO	PV	YES	On board	Power Control	NO	Pros: ● Flexible EV charging Cons: ● Overloading of grid not realized
Proposed	Hybrid	YES	NO	PV	YES	Off board	PV and DC link Power	YES	Pros: ● Provide optimum usage of PV utilization and considering grid overloading, bidirectional power flow for V2V Cons: ● High Cost of ESU installation

7. Conclusions

The EMS for a multiport BEV charging station powered by a hybrid microgrid is proposed in this paper. The proposed EMS maintains the DC bus voltage irrespective of utility grid overloading caused either by the local load or meagerness of PV power. Eleven different modes of the EMS were developed for the proposed microgrid to provide continuous power to the BEV charging point. Moreover, when the utility grid is fully loaded, and irradiation of the PV system is low, BEV charging is delayed or temporarily interrupted. The power demand is managed by the ESU and vehicle-to-vehicle charging. MATLAB/Simulink simulation analyses were performed for the proposed hybrid multiport charging station with EMS, and the system was validated with an experimental study. Based on the observed results using different modes of operation, the proposed EMS strategy shows better performance by maintaining the DC bus power and effectively utilizing PV energy.

Author Contributions: All authors were involved in developing the concept, simulation, and experimental validation and making the article error free and getting a technical outcome for the set investigation work.

Funding: This research received no external funding.

Acknowledgments: Authors like to acknowledge the support and technical expertizes received from the center for Bioenergy and Green Engineering, Department of Energy Technology, Aalborg University, Esbjerg, Denmark. Also, to the Center of Reliable Power Electronics (CORPE) for providing additional technical supports received and made this publication possible.

Conflicts of Interest: The authors declare no conflict of interest.

Abbreviations

V_{PV}	Output voltage of the PV panel
I_{PV}	Output current of the PV panel
P_{PV}	PV power
V_{DTR}	Voltage drawn from the utility grid
I_{DTR}	Current drawn from the utility grid
I_{FB}	Feedback current to the utility grid
I_{S1}	Boost converter current
V_{ESU}	ESU battery voltage
I_{ESU}	ESU battery current
P_{ESU}	Energy storage unit power
I_{ref}	Battery charging current
P_{CS}	Charging station power
P_{UG}	Power drawn from the utility grid
BEV	Battery electric vehicle
G2V	Grid to vehicle
V2V	Vehicle to vehicle
ESU2V	ESU to vehicle
$V_{DC\ BUS}$	DC bus voltage
$P_{DC\ BUS}$	DC bus power
P_{BEV-N}	BEVs power
P_{BEV-K}	Particular BEV power
$P_{PV\ REF-1}$	PV power reference 1
$P_{PV\ REF-2}$	PV power reference 2
$P_{PV\ REF-3}$	PV power reference 3
SOC_{ESU}	SOC of energy storage unit
SOC_{BEV}	SOC of battery electric vehicle
$V_{BEV-1}-V_{BEV-3}$	BEVs' battery voltages
I_{SW}	Isolation switch

References

1. Prakash, J.; Habib, G. A technology-based mass emission factors of gases and aerosol precursor and spatial distribution of emissions from on-road transport sector in India. *Atmos. Environ.* **2018**, *180*, 192–205. [[CrossRef](#)]
2. Fulton, L.; Mejjia, A.; Arioli, M.; Dematera, K.; Lah, O. Climate change mitigation pathways for Southeast Asia: CO2 emissions reduction policies for the energy and transport sectors. *Sustainability* **2017**, *9*, 1160. [[CrossRef](#)]
3. Bose, R.K.; Srinivas chary, V. Policies to Reduce Energy Use and Environmental Emissions in the Transport Sector: A Case of Delhi City. *Energy Policy* **1997**, *25*, 1137–1150. [[CrossRef](#)]
4. Emadi, A.; Lee, Y.J.; Rajashekara, K. Power electronics and motor drives in electric hybrid electric and plug—in hybrid electric vehicles. *IEEE Trans. Ind. Electron.* **2008**, *55*, 2237–2245. [[CrossRef](#)]
5. Wang, C.S.; Stielau, O.H.; Covic, G.A. Design considerations for a contactless electric vehicle battery charger. *IEEE Trans. Ind. Electron.* **2005**, *52*, 1308–1314.
6. Guerrero, J.M.; Loh, P.C.; Lee, T.L. Advanced control architectures for intelligent Microgrids-part II: Power quality, energy storage, and AC/DC Microgrids. *IEEE Trans. Ind. Electron.* **2013**, *60*, 1263–1270. [[CrossRef](#)]
7. Preetham, G.; Shireen, W. Photovoltaic charging station for plug-in hybrid electric vehicles in a smart grid environment. In Proceedings of the IEEE PES Innovative Smart Grid Technologies, Washington, DC, USA, 16–20 January 2012; pp. 1–8.
8. Vaidya, M.; Stefanakos, E.; Krakow, B.; Lamb, H.; Arbogast, T.; Smith, T. Direct DC-DC electric vehicle charging with a grid connected photovoltaic system. In Proceedings of the 25th IEEE Photovoltaic Specialists Conference, Washington, DC, USA, 13–17 May 1996; pp. 1505–1508.
9. Fenton, J.; Hodkinson, R. *Lightweight Electric/Hybrid Vehicle Design*; Elsevier: Amsterdam, The Netherlands, 2001.
10. Ruiz-Rodriguez, F.J.; Hernández, J.C.; Jurado, F. Voltage behaviour in radial distribution systems under the uncertainties of photovoltaic systems and electric vehicle charging loads. *Int. Trans. Electr. Energy Syst.* **2018**, *28*, e2490. [[CrossRef](#)]
11. Yilmaz, M.; Krein, P.T. Review of Charging Power Levels and Infrastructure for Plug-In Electric and Hybrid Vehicles. In Proceedings of the IEEE International Electric Vehicle Conference (IEVC'12), Greenville, SC, USA, 4–8 March 2012.
12. Chen, H.; Hu, Z.; Luo, H.; Qin, J.; Rajagopal, R.; Zhang, H. Design and Planning of a Multiple-charger Multiple-port Charging System for PEV Charging Station. *IEEE Trans. Smart Grid* **2017**, *10*, 173–183. [[CrossRef](#)]
13. Chokkalingam, B.; Padmanaban, S.; Siano, P.; Krishnamoorthy, R.; Selvaraj, R. Real-Time Forecasting of EV Charging Station Scheduling for Smart Energy Systems. *Energies* **2017**, *10*, 377. [[CrossRef](#)]
14. Sanchez-Sutil, F.; Hernández, J.C.; Tobajas, C. Overview of electrical protection requirements for integration of a smart DC node with bidirectional electric vehicle charging stations into existing AC and DC railway grids. *Electric Power Syst. Res.* **2015**, *122*, 104–118. [[CrossRef](#)]
15. Du, Y.; Zhou, X.; Bai, S.; Lukic, S.; Huang, A. Review of non-isolated bi-directional DC-DC converters for plug-in hybrid electric vehicle charge station application at municipal parking decks. In Proceedings of the Applied Power Electronics Conference and Exposition (APEC), Palm Springs, CA, USA, 21–25 February 2010; pp. 1145–1151.
16. Salas, V.; Olias, E.; Barrado, A.; Lazaro, A. Review of the maximum power point tracking algorithms for stand-alone photovoltaic systems. *Sol. Energy Mater. Sol. Cells* **2006**, *90*, 1555–1578. [[CrossRef](#)]
17. Hernandez, J.C.; Sutil, F.S. Electric vehicle charging stations fed by renewable: PV and train regenerative braking. *IEEE Latin Am. Trans.* **2016**, *14*, 3262–3269. [[CrossRef](#)]
18. Pickard, W.F.; Shen, A.Q.; Hansing, N.J. Parking the power: Strategies and physical limitations for bulk energy storage in supply–demand matching on a grid whose input power is provided by intermittent sources. *Renew. Sustain. Energy Rev.* **2009**, *13*, 1934–1945. [[CrossRef](#)]
19. ESRAM, T.; Chapman, P.L. Comparison of photovoltaic array maximum power point tracking techniques. *IEEE Trans. Energy Convers.* **2007**, *22*, 439–449. [[CrossRef](#)]
20. Xiao, B.; Hang, L.; Mei, J.; Riley, C.; Tolbert, L.M.; Ozpineci, B. Modular cascaded H-bridge multilevel PV inverter with distributed MPPT for grid-connected applications. *IEEE Trans. Ind. Appl.* **2015**, *51*, 1722–1731. [[CrossRef](#)]

21. Carrasco, J.M.; Franquelo, G.; Bialasiewicz, T.; Galvan, E.; Guisado, R.C.P.; Prats, A.M.; Le´on, J.I.; Moreno-Alfonso, N. Power-electronic systems for the grid integration of renewable energy sources: A survey. *IEEE Trans. Ind. Electron.* **2006**, *53*, 1002–1016. [[CrossRef](#)]
22. Hamilton, C.; Gamboa, G.; Elmes, J.; Kerley, R.; Arias, A.; Pepper, M.; Shen, J.; Batarseh, I. System architecture of a modular direct-DC PV charging station for plug-in electric vehicles. In Proceedings of the IECON 2010—36th Annual Conference on IEEE Industrial Electronics Society, Glendale, AZ, USA, 7–10 November 2010; pp. 2516–2520.
23. Shaikat, N.; Khan, B.; Ali, S.M.; Mehmood, C.A.; Khan, J.; Farid, U.; Majid, M.; Anwar, S.M.; Jawad, M.; Ullah, Z. A survey on electric vehicle transportation within smart grid system. *Renew. Sustain. Energy Rev.* **2017**, *81*, 1329–1349. [[CrossRef](#)]
24. Fathima, A.H.; Palanisamy, K.; Sanjeevikumar, P.; Umashankar, S. Intelligence-based battery management and economic analysis of an optimized dual-Vanadium Redox Battery (VRB) for a Wind-PV HYBRID SYSTEM. *Energies* **2018**, *11*, 2785. [[CrossRef](#)]
25. Zhao, Z.; Hu, J.; Chen, H. Bus Voltage Control Strategy for Low Voltage DC Microgrid Based on AC Power Grid and Battery. In Proceedings of the 2017 IEEE International Conference on Energy Internet (ICEI), Beijing, China, 17–21 April 2017; pp. 349–354.
26. Khajehoddin, S.A.; Karimi-Ghartemani, M.; Jain, P.K.; Bakhshai, A. DC-bus design and control for a single-phase grid-connected renewable converter with a small energy storage component. *IEEE Trans. Power Electron.* **2013**, *28*, 3245–3254. [[CrossRef](#)]
27. Li, X.; Guo, L.; Wang, C.; Zhang, S.; Rong, Y.; Feng, Y.; Li, Y. Robust and autonomous DC bus voltage control and stability analysis for a DC microgrid. In Proceedings of the 2016 IEEE 8th International Power Electronics and Motion Control Conference (IPEMC-ECCE Asia), Hefei, China, 22–26 May 2016; pp. 3708–3714.
28. Chen, D.; Xu, L.; Yao, L. DC voltage variation based autonomous control of DC microgrids. *IEEE Trans. Power Deliv.* **2013**, *28*, 637–648. [[CrossRef](#)]
29. Yoon, S.G.; Kang, S.G. Economic microgrid planning algorithm with electric vehicle charging demands. *Energies* **2017**, *10*, 1487. [[CrossRef](#)]
30. Ul-Haq, A.; Cecati, C.; Al-Ammar, E.A. Modeling of a Photovoltaic-Powered Electric Vehicle Charging Station with Vehicle-to-Grid Implementation. *Energies* **2016**, *10*, 4. [[CrossRef](#)]
31. Zhou, D.; Al-Durra, A.; Matraji, I.; Ravey, A.; Gao, F. Online Energy Management Strategy of Fuel Cell Hybrid Electric Vehicles: A Fractional-Order Extremum Seeking Method. *IEEE Trans. Ind. Electron.* **2018**, *65*, 6787–6799. [[CrossRef](#)]
32. Dragicevic, T.; Guerrero, J.M.; Vasquez, J.C.; Skrlec, D. Supervisory control of an adaptive-droop regulated DC microgrid with battery management capability. *IEEE Trans. Power Electron.* **2014**, *29*, 695–706. [[CrossRef](#)]
33. Demirok, E.; Gonzalez, P.C.; Frederiksen, K.H.; Sera, D.; Rodriguez, P.; Teodorescu, R. Local reactive power control methods for overvoltage prevention of distributed solar inverters in low-voltage grids. *IEEE J. Photovolt.* **2011**, *1*, 174–182. [[CrossRef](#)]
34. Karimi-Ghartemani, M.; Khajehoddin, S.A.; Jain, P.; Bakhshai, A. A systematic approach to DC-bus control design in single-phase grid-connected renewable converters. *IEEE Trans. Power Electron.* **2013**, *28*, 3158–3166. [[CrossRef](#)]
35. Haghbin, S.; Lundmark, S.; Alakula, M.; Carlson, O. Grid-connected integrated battery chargers in vehicle applications: Review and new solution. *IEEE Trans. Ind. Electron.* **2013**, *60*, 459–473. [[CrossRef](#)]
36. Dallinger, D.; Wietschel, M. Grid integration of intermittent renewable energy sources using price-responsive plug-in electric vehicles. *Renew. Sustain. Energy Rev.* **2012**, *16*, 3370–3382. [[CrossRef](#)]
37. Rahman, I.; Vasant, P.M.; Singh, B.S.M.; Abdullah-Al-Wadud, M.; Adnan, N. Review of recent trends in optimization techniques for plug-in hybrid, and electric vehicle charging infrastructures. *Renew. Sustain. Energy Rev.* **2016**, *58*, 1039–1047. [[CrossRef](#)]
38. Escudero-Garzas, J.J.; Seco-Granados, G. Charging station selection optimization for plug-in electric vehicles: An oligopolistic game-theoretic framework. In Proceedings of the Innovative Smart Grid Technologies, Washington, DC, USA, 16–20 January 2012; pp. 1–8.
39. Wang, M.; Ismail, M.; Zhang, R.; Shen, X.S.; Serpedin, E.; Qaraqe, K. A semi-distributed V2V fast charging strategy based on price control. In Proceedings of the 2014 IEEE Global Communications Conference, Austin, TX, USA, 8–12 December 2014; pp. 4550–4555.

40. Hernández, J.C.; Sanchez-Sutil, F.; Vidal, P.G.; Rus-Casas, C. Primary frequency control and dynamic grid support for vehicle-to-grid in transmission systems. *Int. J. Electr. Power Energy Syst.* **2018**, *100*, 152–166. [[CrossRef](#)]
41. Bhatti, A.R.; Salam, Z.; Ashique, H. Electric vehicle charging using photovoltaic based microgrid for remote islands. *Energy Procedia* **2016**, *103*, 213–218. [[CrossRef](#)]
42. Tran, V.T.; Sutanto, D.; Muttaqi, K.M. The state of the art of battery charging infrastructure for electrical vehicles: Topologies, power control strategies, and future trend. In Proceedings of the 2017 Australasian Universities Power Engineering Conference (AUPEC), Melbourne, VIC, Australia, 19–22 November 2017; pp. 1–6.
43. Goli, P.; Shireen, W. PV Integrated Smart Charging of PHEVs Based on DC Link Voltage Sensing. *IEEE Trans. Smart Grid* **2014**, *5*, 1421–1428. [[CrossRef](#)]
44. Sbordone, D.; Bertini, I.; Di Pietra, B.; Falvo, M.C.; Genovese, A.; Martirano, L. EV fast charging stations and energy storage technologies: A real implementation in the smart micro grid paradigm. *Electr. Power Syst. Res.* **2015**, *120*, 96–108. [[CrossRef](#)]
45. Nagarajan, A.; Shireen, W. Grid connected residential photovoltaic energy systems with Plug-In Hybrid electric Vehicles (PHEV) as energy storage. In Proceedings of the IEEE PES General Meeting, Providence, RI, USA, 25–29 July 2010; pp. 1–5.



© 2019 by the authors. Licensee MDPI, Basel, Switzerland. This article is an open access article distributed under the terms and conditions of the Creative Commons Attribution (CC BY) license (<http://creativecommons.org/licenses/by/4.0/>).